Computers, Materials & Continua

Tech Science Press

https://doi.org/10.32604/cmc.2026.082467

ARTICLE

A Hybrid Learning Framework for Underwater Image Enhancement

Sami Ullah[1,2], **Najmul Hassan**[2], **Naeem Bhatti**[2] and **Asad Saleem**[1,*]

[1]School of Electronic Engineering and Intelligent Manufacturing, Anhui Xinhua University, Hefei, China
[2]COMSIP LAB, Department of Electronics, Quaid-i-Azam University, Islamabad, Pakistan

*Corresponding Author: Asad Saleem. Email: asadalvi64@yahoo.com

Received: 16 March 2026; Accepted: 07 May 2026; Published: 15 June 2026

ABSTRACT: Underwater imaging facilitates the exploration of the underwater environment. However, irregular optical absorption and light scattering in water, ranging from clear to highly turbid conditions, often result in low visibility, color distortion, and blurriness in underwater images (UWIs). Conventional UWI enhancement methods are limited by inefficient physical modeling, while deep learning-based approaches are constrained by the scarcity of paired training datasets. In this work, we propose a hybrid learning framework for UWI enhancement that leverages the usefulness of both conventional and deep learning-based techniques. At first, we preprocess the UWIs using a revised underwater physical model, contrast adaptive histogram equalization (CLAHE), gamma correction (GC), and single-scale retinex (SSR) techniques. These preprocessed images, together with the corresponding raw UWIs, are then used to train a convolutional neural network (CNN) to generate confidence maps for each enhancement result. Simultaneously, we employ a second CNN-based feature transformation network (FTN), which consists of four feature transformation units (FTU). We train each FTU using a raw UWI and its corresponding preprocessed image to obtain confidence maps. In order to exploit the complementary strengths of the revised underwater physical model confidence and refined maps (from CNN and FTN), we use them to scale the remaining information maps. Finally, we perform additive fusion of the scaled maps to obtain enhanced UWI. Experiments on diverse UWI datasets, including the real-world image enhancement (RIE) dataset (which contains a variety of degradation effects with greenish, bluish, and green-bluish tones), the underwater image enhancement benchmark (UIEB), and the enhancement of underwater visual perception (EUVP) dataset, demonstrate the enhanced generality and effectiveness of the proposed approach.

KEYWORDS: Underwater image restoration; physical model; CNNs; confidence maps; refined maps

1 Introduction

The deep sea areas are house of various resources and their exploration needs advanced tools. Developing such tools invite research community to invest their efforts with a focus on understanding underwater environment [1]. As a result, multi-disciplinary research areas such as biological oceanography, geographical and oceanic archaeological exploration, etc. have been emerged in literature. As the underwater environment is not a favorable habitat for humans therefore its exploration pose various challenges. Underwater imaging is an alternate providing the underwater images (UWIs) of environment avoiding physical intervention. While underwater imaging is an effective method, however UWIs are found to suffer from issues such as low visibility, color cast, and blurriness. Since 70% of the Earth's surface is underwater, restoring and enhancing the visual information in the captured UWIs is an important and challenging area of research.

In literature, both conventional and deep learning-based approaches have been presented targeting underwater image enhancement. He et al. present a dark channel prior (DCP) based technique for UWI

enhancement [2]. The DCP method estimates the atmospheric light and transmission maps, and used them in UWI enhancement. Recognizing the effectiveness and simplicity of DCP, Galdran et al. [3] extended it as red channel prior in an attempt to recover the shorter wavelengths that are highly attenuated. Moreover, Drews et al. [4] present the underwater dark channel prior. They perform color restoration using green and blue channels. Although the DCP-based approaches are found to be simple and easy to implement, however they are highly dependent upon prior knowledge (weather conditions) of UWIs, which marginalized their generality and mostly suffer from red channel artifacts [5]. The approaches such as the histogram-equalization-based, white balance-based, retinex-based, and fusion-based approaches do not take into account the image formation model, are also explored in literature. The histogram-based techniques such as histogram equalization [6], contrast adaptive histogram equalization [7] and histograms stretching [8] are found effective in improving the global visibility of UWIs. Achieving UWI enhancement, Iqbal et al. [9] and Ancuti et al. [10] perform pixel-wise modifications. These techniques are found to perform over enhancement as they do not take into account the optical model [10]. The retinex-based techniques [11–13], histograms stretching [14,15] and fusion-based techniques [16,17] do not take into account the prior knowledge.

In [16], Ancuti et al. obtain an enhanced UWI merging various processed versions of UWI (enhanced version, color restored version) using a multiscale fusion strategy. Fu et al. decompose the UWI into reflectance and illumination components, they enhance these components using retinex-based technique and combine them to obtain enhanced UWIs [18]. Fusion-based techniques perform UWI restoration and enhancement well but are computationally inefficient.

Recently, various approaches have been presented using deep learning algorithms. Li et al. present a deep neural network which performs color shift and enhance the degraded components [19]. Further extending their work, they present a semi-supervised learning WaterGAN deep network [20]. They achieve UWI restoration in two steps. At first, they estimate UWIs from in-air images along with depth. Next, they train the enhancement model (that is UWCNN) on 10 water types described in [21]. The WaterGAN achieves good overall results, but its performance suffers in the case of diverse underwater scenes. This shortcoming lies in the use of a synthetic data set that does not represent the real UWIs appropriately. Among other reasons of the deep learning-based techniques to be outperformed by the conventional techniques in case of UWIs is the lack of a large amount of real data. In [22], Li et al. present a deep learning model called the water-net model. Instead of using the real UWIs, they preprocess the UWIs using histogram equalization (HE), gamma correction (GC) and white balancing (WB) to preprocess the UWIs. The HE enhances the visual information at the cost of noise, GC attempts to reduce noise, while the WB overcomes color artifacts. The preprocessed images are fed to the water-net model, which comprises of a CNN and feature transformation units (FTUs). The CNN provides three confidence maps, while the FTUs refine the preprocessed images. The outputs of CNNs and FTNs are combined to produce enhanced UWIs. Moreover, they use a pretrained VGG-19 with ReLU activation layers to characterize the perception loss. We note that the preprocessing of UWIs by the conventional techniques (HE, GC, and WB) limit the generalization of water-net model as they do not consider the particular image formation of underwater imaging.

In this work, we propose a physical model-based convolutional neural network (PM-CNN). In order to achieve preprocessing of UWIs, we use RUFIM with non-physical model-based techniques: the GC, contrast-limited adaptive histogram equalization (CLAHE), and single-scale retinex (SSR). The preprocessed images are further processed using the CNN and feature transformation networks as of the water-net model. The CLAHE performs image enhancement by applying a clip limit in order to avoid over-enhancement. The SSR performs color restoration of UWIs using the Retinex theory. The CNN of our PM-CNN model generates four confidence maps (CMs) corresponding to each input preprocessed image. Additionally, we design four FTNs that refine the preprocessed images, where each FTN is fed with the raw UWI along with a

preprocessed image. The RUFIM FTN refined output map is then propagated into the CLAHE, GC, and SSR-based refined FTN maps. This incorporation of RUFIM enables our model to deal with the diverse scenes of underwater images effectively, preventing both under-enhancement and over-enhancement, and increasing its generalization. The framework of the proposed hybrid image-enhancement model is given in Fig. 1. We list our contributions in this work as follows:

- We present a UWI enhancement framework, which incorporates three types of processes: the conventional approaches, the physical model-based, and the deep learning-based processes. This incorporation, particularly of the physical model enhances the generalization of the model.
- The proposed framework involves a physical model based convolutional neural network and a feature transform network, which are trained using pre-processed UWIs. We introduce a refinement of the networks output maps by scaling them using the physical model-based network map before their fusion to obtain enhanced UWI.
- We present the effectiveness of the single-scale retinex, gamma correction and contrast-limited adaptive histogram equalization techniques in comparison to the traditional white balance for enhancing UWIs, incorporating them in a learning framework.

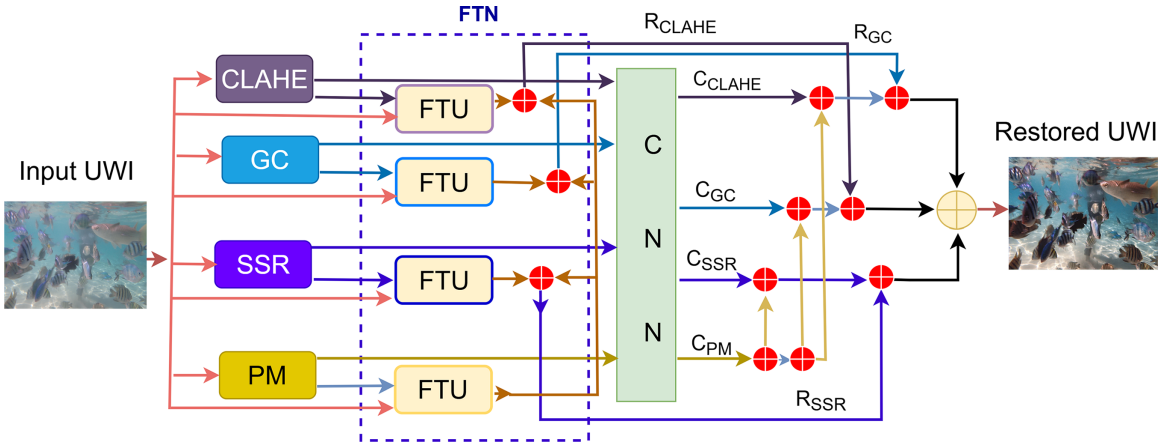

Figure 1: Framework of the proposed hybrid image-enhancement model.

The rest of the paper is organized as follows. Section 2 reviews related work on UWI enhancement. Section 3 describes the datasets used for training and evaluation. Section 4 presents the proposed model, including the preprocessing techniques and the training protocol. Section 5 presents the experimental results, including the ablation study. Finally, Section 6 concludes the paper.

2 Related Work

We categorize the literature on UWI enhancement techniques into four distinct groups: conventional techniques based on PM, conventional techniques not based on PM, deep learning techniques that utilize PM, and deep learning techniques that do not utilize PM. Additionally, we emphasize the importance of the underwater PM within each of these approach categories.

2.1 Conventional Techniques Based on Physical Models

The PM mostly estimates the global transmission and veiling light. Zhou et al. [23] exploit the backscatter technique for the improvement of contrast and removing color casts of UWIs. Liang et al. [5] present three estimation processes: color balance, a discernment function that uses linear saturation-based

details restoration, and contrast restoration. Wang et al. [24] present the adaptive attenuation curve prior-based UWI enhancement technique. Their technique attempts to model the attenuation process of light for various underwater environments. Berman et al. [25] address wavelength-dependent attenuation by using a haze line. They adapted the method of single UWI restoration. Li et al. [19] adapt the minimum information loss principle and histogram distribution before enhancing the UWIs. Yuan et al. [26] address color cast and blurry details in UWIs by using the fusion strategy. They attempt to eliminate global fog in the UWIs using contrast-guide dark channels prior. Moreover, they use morphology extraction and color compensation methods to enhance brightness and chroma receptively. Peng and Cosman [27] enhance UWIs using depth estimation based on image blurriness and light absorption. Akkaynak and Treibitz [28] collect images at various distances (2, 5, 10 m) in the Mediterranean and the Red Sea and keep these images as RGB-d dataset. They revise the traditional underwater image formation model by using the depth (distance) information (TUIFM). Ignoring the depth (effect of the scene on camera distance) by TUIFM led to the unsatisfactory restoration of UWI. However, the revised model of Akkaynak considers 10 classes of Jerlov water types. They use the attenuation coefficient β_c for each water type in the restoration of the UWIs. However, Ullah et al. [29] investigate that the RUIFM does not take into account the diversity of β_c representing each water type. In order to attain a precise β_c they further classify each water type into low, medium, and high bands. Considering the diverse attenuation representation and based on RUIFM, they propose a diverse underwater image formation model (DUIFM), which can restore the UWIs captured in a variety of underwater environments. Most of the aforementioned techniques use physical and do not often apply extra information, which is the depth of the UWIs. Thus, the estimation process may often lead to wrong restoration. Moreover, Akkaynak and Treibitz [28] and Ullah et al. [29] adopt a comprehensive underwater image formation model in which they encounter the depth information of UWIs, as the optical properties of UWIs are highly depth dependent. Thus, they achieve better performance in terms of restoration and enhancement of UWIs. However, the lack of underwater RGB-d datasets limits the application of these models.

2.2 Conventional Techniques Not Based on Physical Models

Nonphysical model-based techniques directly modify pixel values to enhance the visual appearance of UWIs [30]. Yuan et al. [31] present contour bougie morphology to enhance UWIs. They apply two structuring elements with different sizes as convolution windows to perform multiple morphological operations for enhancing scene contours and improving UWI visibility. Zhuang et al. [11] present a Bayesian retinex technique that uses multi-order gradient priors of reflectance to enhance single UWIs. Zhuang et al. [32] used minimum color loss and maximum attenuation map-guided fusion to locally adjust colors and details. They perform adaptive contrast adjustment and color balance strategy, integral and squared integral maps in CIELAB color space. Zhang et al. [33] present a weighted wavelet visual perceptual fusion (WWPF) technique that fuses attenuation-map-guided color correction, wavelet-based visual perception, and wavelet-based visual perception for UWIs color correction and enhancement. The non-physical model-based methods often set parameters by empirical values. They can improve the contrast and color of UWIs, but may not consistently maintain enhancement and could give rise to either inadequate or excessive enhancement due to irregular IOP of various underwater scenes [34].

2.3 Deep Learning Techniques That Utilize Physical Models

In recent years, significant advancement has been found in deep learning models for low-level vision problems [35]. Mostly the models are trained using synthetic datasets. However, the physical model of UWI for extremely different from other image formation models (daytime fogy images, nighttime hazy images),

therefore synthesizing UWIs does not match the real UWIs. Moreover, the enhancement and restoration of UWIs by deep learning model is still behind the conventional technique [36]. Li et al. [20] present WaterGAN which is a generative adversarial network (GAN). It simulates UWIs based on the physical underwater imaging model. It generates paired synthetic UWIs and their corresponding clean images. These pairs are used to train CNN for UWI enhancement. However, the physical model is used only for data synthesis, not for restoration, thus their model does not provide generalized results. Li et al. [21] attempt to guide the U-Net by the IOP of water. They use underwater image formation model equations as part of the loss function. Incorporating the simplified model in the U-Net, they achieve, to some extent, realistic enhancement results of UWIs. Since they use a simplified underwater image formation model, they do not achieve satisfactory results. Guo et al. [37] introduce a dual-branch network. One branch encounters the underwater physical properties of light while the other performs standard deep learning enhancement. The final result fuses the outputs of both branches, using attention mechanisms guided by the underwater image formation model. Liu et al. [38] integrate the RUFIM and neural network to get the benefit of both approaches. The RUFIM guides the network learning, while the GAN is used for coefficient estimation. Chang et al. [39] integrate illumination-aware feature extraction, transmission-guided multi-scale optimization, and spatial feature aggregation to enhance underwater images. They separate illumination and reflectance information in order to refine the features through learnable residual structures guided by transmission maps. The reported results demonstrate a reduced distortion while preserving important image details. The deep learning techniques that are based on physical models offer promising enhancement over the pure deep learning model for UWI enhancement. More realistic and generalized results can be achieved by embedding knowledge of underwater light propagation into network architectures and loss functions. In the proposed work we attempt to bridge the gap between theoretical accuracy and practical application by combining physical model and data-driven methods. The combination of both makes our model particularly powerful for restoration.

2.4 Deep Learning Techniques That Do Not Utilize Physical Models

The techniques that only exploit the strength of neural networks and do not consider other additional knowledge are called pure deep learning techniques. These techniques are computationally more efficient than the non-pure techniques, but these techniques do not perform realistic enhancement of UWIs. Moreover, these techniques required huge paired data, which is scarce in the case of UWIs. Fabbri et al. [40] use a purely data-driven U-Net architecture for UWI enhancement. They use the encoder structure for feature extraction and the decoder for enhancement of UWIs. The technique learns low- to high-level features from UWIs. Li et al. [41] present a GAN-based Ucolor model in which the generator directly restores the color based on the training dataset, while the discriminator attempts to enhance UWIs to look natural. Islam et al. [42] present EnhanceGAN, which uses a generator-discriminator structure. It performs learning a mapping between low-quality and high-quality UWIs. The generator enhances the UWIs, and the discriminator learns to differentiate real high-quality images from enhanced ones. The network is trained in an adversarial fashion, and the focus is purely on learning from data without considering any physical models of light propagation. The deep learning-based techniques use end-to-end CNNs or GANs to enhance UWIs without using the physical models [43,40]. It is observed that without considering the underwater image formation model, the data-driven techniques cannot often achieve a proper enhancement of UWIs and sometimes require a large amount of reference dataset to train the model [44]. Such a scenario signifies the image formation model. Experimentally, it is widely investigated every group has its benefit in certain paradigms, therefore combining several techniques can provide better enhancement of UWIs captured in a variety of underwater environments. Therefore in the proposed work, we train our model using techniques from each explained group in Sections 2.1–2.4.

3 Datasets for Underwater Image Enhancement and Evaluation

To comprehensively assess the effectiveness of the proposed approach, several publicly available underwater image datasets are utilized. A brief description of each dataset is provided below.

UIEB (Underwater Image Enhancement Benchmark)

The UIEB dataset contains 950 real underwater images captured under diverse environmental conditions. Among these, 890 images are paired with high-quality reference images, while the remaining 60 images are considered challenging samples without reliable ground-truth references. The dataset was introduced alongside the Water-Net framework and has since become a standard benchmark for evaluating underwater image enhancement algorithms. In line with common experimental protocols, 800 images are used for training, and 90 images are reserved for testing (commonly referred to as the T-90 subset).

EUVP-T515 (Enhancing Underwater Visual Perception)

The EUVP dataset includes approximately 20,000 underwater images exhibiting varying degrees of visual degradation. It comprises both paired (12,000 images) and unpaired (8000 images) samples. For evaluation purposes, a subset of 515 images is selected, referred to as EUVP-T515, following previously reported experimental settings in the literature.

RUIE-T78 (Real-World Underwater Image Enhancement)

The RUIE dataset consists of real underwater images categorized into three subsets: UCCS (underwater color cast scenes), UIQS (images captured under different water quality conditions), and UHTS (underwater object detection scenarios). To ensure balanced evaluation, 26 images are selected from each subset, forming a total of 78 test images, which we denote as RUIE-T78 [45].

4 Proposed Approach

The proposed approach uses contrast-limited adaptive histogram equalization (CLAHE), gamma correction (GC), single scale Retinex (SSR), and revised underwater image formation model (RUIFM) to preprocess the images at the first stage and then they are used for extracting the features by a CNN and feature transform network (FTN). First, we describe the preprocessing techniques and then give the architecture of the proposed model along with the loss function used for training.

4.1 Preprocessing Techniques

For an input underwater image I, at first we obtain multiple enhanced versions $I_{CLAHE}, I_{GC}, I_{SSR}, I_{PM}$ using different preprocessing techniques. where I_{CLAHE} represents the contrast-enhanced image using CLAHE, I_{GC} is the gamma-corrected image, I_{SSR} is obtained using Single Scale Retinex and I_{PM} denotes the output of the Revised Underwater Image Formation Model (RUIFM). These preprocessed images provide diverse representations by capturing complementary visual characteristics such as contrast, illumination, and color correction. In the following, we give a description of the conventional processing techniques, CLAHE, GC, SSR and RUIFM, respectively.

Contrast Limited Adaptive Histogram Equalization: In [46], Kim et al. presented a histogram equalization technique introducing a clip limit. The CLAHE works by decomposing an image into small disjoint contextual regions called patches. An arbitrary image of size $Z \times Z$ has the size of each patch $m \times m$ (usually the size of tile: 8×8 is used in practice). The technique constructs the histogram of each patch and applies a clip limit calculated as $CL = N_{cl} \times N_{avg}$, where N_{cl} is the normalized contrast limit, which is set manually (in this work $N_{cl} = 0.002$ is used). N_{avg} is the average number of pixels for each gray level in patches calculated as $N_{gray} = N_x \times N_y$. The N_{gray} represents the number of gray levels in a patch, N_x and N_y are the number

of pixels in the x and y dimensions of a patch, respectively. An arbitrary image $I_{UWI}(m,n)$ of size $M \times N$ having maximum intensity level L is processed as:

$$I_{CLAHE}(m,n) = T(I(m,n)) = \frac{(L-1)}{MN}\sum_{j}^{K} f_j \tag{1}$$

The f_j is the frequency of intensity level j, which is constrained by the contrast limit CL (described above). For details, we refer to [13,47,48], where the authors explored the CLAHE for day time fogy image enhancement, night time fogy image enhancement and for UWIs enhancement, respectively.

Gamma Correction: Due to light scattering in underwater environment the brightness in UWIs is not uniform. We use the gamma correction to achieve brightness equalization. The brightness equalized image I_{GC} is obtained as:

$$I_{GC} = (I_{input})^{\gamma} \tag{2}$$

where I_{input} is the input normalized image between 0 and 1, whereas the γ is correction parameter. The human visual system perceives brightness in a nonlinear manner and is more sensitive to changes in dark areas than in bright areas. The *GC* redistributes the intensity levels to make the image appear more natural. Moreover, in the underwater environments, red light is absorbed quickly leading to a predominance of blue and green hues. The equalization of brightness also enhances these colors for better visual interpretation. It is observed in our experiments that by applying a suitable γ value (typically less than 1 for UWIs), the *GC* brings out details in darker areas of the image.

Single Scale Retinex: The retinex theory simulates human visual perception in order to improve the visibility of details. It considers an underwater image $I(x,y)$ as a product of reflectance $R(x,y)$ and luminance $L(x,y)$ components as:

$$I(x,y) = R(x,y).L(x,y) \tag{3}$$

The SSR-processed UWI is obtained as

$$SSR_{uw}(x,y) = I(x,y) - L(x,y), \tag{4}$$

where $L(x,y)$ is an estimation of the luminance component [49] and is obtained using a low-pass Gaussian filter $G(x,y)$ as:

$$I_{SSR}(x,y) = G(x,y)I(x,y) \tag{5}$$

Note that it models the smooth and large-scale variations in the image.

Revised Underwater Image Formation Model: The RUIFM performs UWI restoration, preventing the process from under or over-enhancement. It models the captured image I_c from camera as:

$$I_c(x) = A_c(x)e^{-\beta_c^D(V_D).z} + B_c(1 - e^{-\beta_c^B(V_B).z}) \tag{6}$$

where A_c, i.e., (I_{PM}) is the scene to be captured and attenuated by forward scattering $(e^{-}\beta_c^D(V_D).z)$. The term $A_c(x)e^{-\beta_c^D(V_D).z}$ collectively represents forward scattering. $V_D = z, \rho, E, S_c, \beta_c$, $vB = E, S_c, \beta_c$. z is the object to camera distance and ρ is the reflectance of the object. E represents the irradiance of the scene and S_c is the sensor spectral response. The B_c is the ambient light. The model also takes into account the values

of β_c based on the distance between the object and camera in meters as z = 1, 2, 4, and 5 m. The restored UWI is obtained as:

$$I_{PM} = (I_c - B_c)e^{-\beta_c^D(V_D).z} + (B_c e^{(\beta_c^D(V_D)-\beta_c^B(V_B))z}) \tag{7}$$

The confidence map corresponding to I_{PM} is used to guide the remaining maps.

4.2 Architecture of the Proposed Model

Fig. 2 gives the architecture of the proposed model, which consists of two networks (CNN and FTN) working in parallel. The CNN is designed to produce four confidence maps corresponding to each preprocessed input image. Note that the CNN takes the original UWI along with the CLAHE, GC, SSR and RUIFM processed input images. The FTN consists of four feature transform units (FTUs). A FTU processes a preprocessed image using its original UWI and provides a refined map. In CNN, we set the kernel size of the first four consecutive layers, i.e., 1–4 as: 7 × 7, 5 × 5, 3 × 3, 1 × 1, respectively. The same kernel sizes are used in next four, i.e., 5–8 layers, while for the last two layers (9 and 10) kernel sizes are set as 3 × 3. The first nine layers use the ReLU activation function, while the last layer uses the sigmoid activation function, as we require a bounded output range in our confidence maps. In contrast to the water-net model in [22,50] (where they use eight layers in CNN and three FTUs), we use ten layers and four FTUs. The water-net model [22] relies solely on non-physical preprocessing methods such as CLAHE, GC, and white balance, whereas we incorporate both physical and non-physical priors. Specifically, we replace the white balance technique with single scale retinex (SSR) and introduce the RUIFM as a preprocessing step with an additional FTU. In turn, the extended CNN generates the confidence maps for each preprocessed input. Furthermore, in contrast to the single-stage fusion of water-net model, our model employs a two-stage fusion strategy. In the first stage, the confidence map and the refined map of RUIFM are utilized to guide and scale the remaining confidence and refined maps resulting in more effective feature integration. Moreover, the extended CNN layers allow our network to achieve in depth processing providing more powerful confidence maps.

Confidence Map Estimation: Each preprocessed image is passed through a convolutional neural network $f_\theta(\cdot)$ to estimate pixel-wise confidence maps as

$$\{C_{PM}, C_{CLAHE}, C_{GC}, C_{SSR}\} = f_\theta(I_{PM}, I_{CLAHE}, I_{GC}, I_{SSR}) \tag{8}$$

where $C_k \in \mathbb{R}^{H\times W}$ denotes the confidence map corresponding to the k-th input image. Each confidence map assigns a weight to every pixel, indicating its contribution to the final enhanced image. The confidence maps C_{CLAHE}, C_{GC} and C_{SSR} are further scaled using physical model map C_{PM} as:

$$\{C_{CLAHE}, C_{GC}, C_{SSR}\} = (C_k \odot C_{PM}), \quad k \in \{CLAHE, GC, SSR\} \tag{9}$$

where $\odot$ represents pixel-wise multiplication.

Refine Map Estimation: Each of the four FTUs in FTN provides a refined map as:

$$\{R_{CLAHE}, R_{GC}, R_{SSR}, R_{PM}\} = f_\theta(I_k, I), \quad k \in \{CLAHE, GC, SSR\} \tag{10}$$

The FTUs attempt to decrease the color artifacts introduced by the *CLAHE*, *GC*, and *SSR* techniques. In order to mitigate the refined maps from under or over enhancement we further scale the maps $R_{CLAHE}, R_{GC}, R_{SSR}$ using the physical model refined map R_{PM} as

$$\{R_{CLAHE}, R_{GC}, R_{SSR}\} = (R_k \odot R_{PM}), \quad k \in \{CLAHE, GC, SSR\} \tag{11}$$

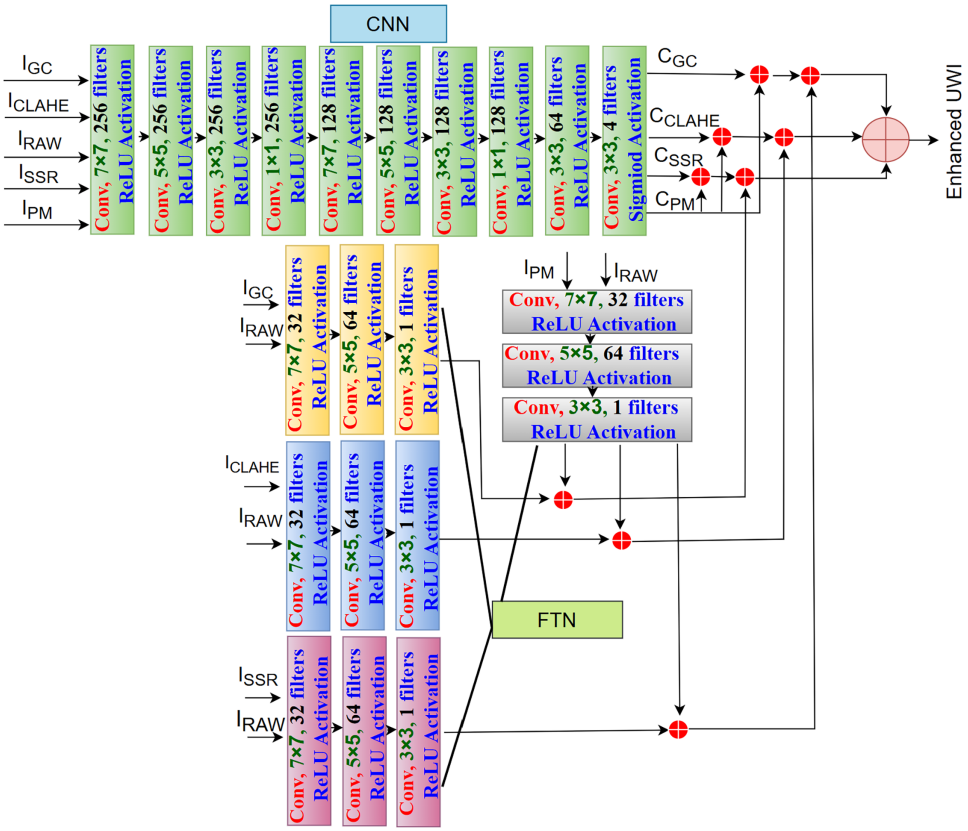

Figure 2: Overall architecture of the proposed hybrid image-enhancement model.

We further scale the scaled refined maps ($R_{CLAHE}, R_{GC}, R_{SSR}$) with their corresponding scaled confidence maps (C_{CLAHE}, C_{GC}, C_{SSR}) and obtain the enhanced maps as:

$$E_{CLAHE} = R_{CLAHE} \odot C_{CLAHE}, \tag{12}$$

$$E_{GC} = R_{GC} \odot C_{GC}, \tag{13}$$

$$E_{SSR} = R_{SSR} \odot C_{SSR} \tag{14}$$

In order to obtain the final enhanced image, we perform additive fusion of enhanced maps E_{CLAHE}, E_{GC}, and E_{SSR} as:

$$E_{UWI} = E_{CLAHE} + E_{GC} + E_{SSR} \tag{15}$$

To train our networks, we apply the loss function used in the waternet model [22] given as:

$$L = \frac{1}{NHB} \sum_{i=1}^{Q} \left\| \sigma_j E^i_{UWIs} - \sigma_j R^i_{UWIs} \right\| \tag{16}$$

where Q, N, H, and B represent the batch size of input UWIs, number, height, and width, respectively. The E_{UWIs} and R_{UWIs} represent the enhanced UWIs and the ground truth- reference images. The σ_j indicates the j_{th} convolution layer, which learns feature maps from both the E_{UWIs} and R_{UWIs}. The loss function computes the difference between these feature maps, encouraging the enhanced image to preserve perceptual

characteristics similar to the reference image. The loss function is used to train the networks through optimization procedures and back-propagation until the minimum loss is achieved, avoiding overfitting.

The extended CNN, along with the four FTUs in FTN, increases the enhancement generality of the proposed model. The improved performance of the proposed architecture on four different challenging datasets validates its enhanced generality, which is presented and discussed in Section 5.

4.3 Training Procedure

Representative traditional and learning-based comparison baselines used in this study include Fusion, ACDC, MLLE, and PUIE [51–54]. More recent deep enhancement baselines include TACL, NU2Net, and CCL-Net [55–57]. Following the training and evaluation protocol of CCL-Net, we use 800 images of the UIEB dataset for training and 90 images, EUVP-T515, RUIE-T78, and RUIE for performance evaluation.

5 Experimental Results

Additional recent baselines considered in the qualitative comparisons include OUNet-JL, WFAC, CLIP-UIE, and U-shape Transformer [58–61]. We carried out experiments on the publicly available UWI datasets of UIEB[1], EUVP[2], the RUIE[3] benchmark introduced in [62], and RUIE [45], which demonstrates the generalization of the proposed approach regarding the UWI enhancement. The RUIE [62] dataset encompasses a wide range of underwater conditions that can be approximately associated with Jerlov water types. Specifically, clear scenes correspond to Type I–IB waters with low turbidity, while more degraded and turbid scenes align with Type II–III waters, characterized by increased scattering and absorption. This diversity enables a comprehensive evaluation of the proposed hybrid model under varying optical conditions. In Figs. 3 and 4, we provide visual results of the proposed model and of the existing approaches: Fusion [51], WaterNet [22], HLRP [32], improved-Retinex [49], and ACDC [52] on RIE dataset images that contain challenging samples of UWIs. Whereas, Figs. 5 and 6 give the visual results on sample images from the EUVP-T515 and UIEB-T90 datasets. A careful comparison of the visual results (given in Figs. 3–7) reveals the generality and effectiveness of the proposed model in terms of restoring and enhancing the UWIs taken in diverse environments. Several competing methods either over-enhance the scene or introduce unnatural saturation, particularly in foreground objects. In some cases, fine textures become overly sharpened or slightly blurred. The proposed method restores stable colors while maintaining consistent contrast and preserving object boundaries without introducing visible artifacts. Fig. 6 presents a qualitative comparison of representative UIEB-T90 samples exhibiting strong greenish and bluish color casts. The raw images suffer from severe wavelength-dependent attenuation, which significantly degrades visibility. Traditional UIE approaches such as Fusion, SMBL, MLLE, WWPF, and WFAC improve global brightness and contrast, but they may still retain noticeable color imbalance in challenging regions. Note that the approach of HLRP [32] introduces blurriness, while the approaches of ACDC [52] and improve Retinex [49] introduce color distortion. UWCNN and WaterNet provide stronger color compensation but occasionally produce over-saturated outputs and artificial tonal shifts. More recent deep learning methods, including PUIE, TACL, NU2Net, CLIP-UIE, U-shape, CCL-Net, and OUNet-JL, preserve structural details more effectively; however, residual color bias and local over-enhancement remain visible in challenging regions. For a fair comparison, we executed the publicly available codes of the compared methods, where available, under the same evaluation setting. The proposed model achieves more balanced color restoration by reducing the dominance of green and blue while maintaining comparable visibility and structural clarity. Compared

[1] http://smartdsp.xmu.edu.cn/underwater.html
[2] https://irvlab.dl.umn.edu/resources/euvp-dataset
[3] https://github.com/agaldran/UnderWater

with recent baselines, the improvement is moderate but consistent, mainly reflected in improved color normalization and fewer visible enhancement artifacts in challenging regions. Fig. 7 further compares the methods on the Challenging-T60 subset, which contains severely degraded underwater images with strong color shifts, scattering, and low visibility. Some methods introduce color artifacts, produce overly dark or saturated results, or show limited ability to recover sufficient contrast. In comparison, the proposed method provides more uniform illumination and better preserves important scene structures under these challenging conditions.

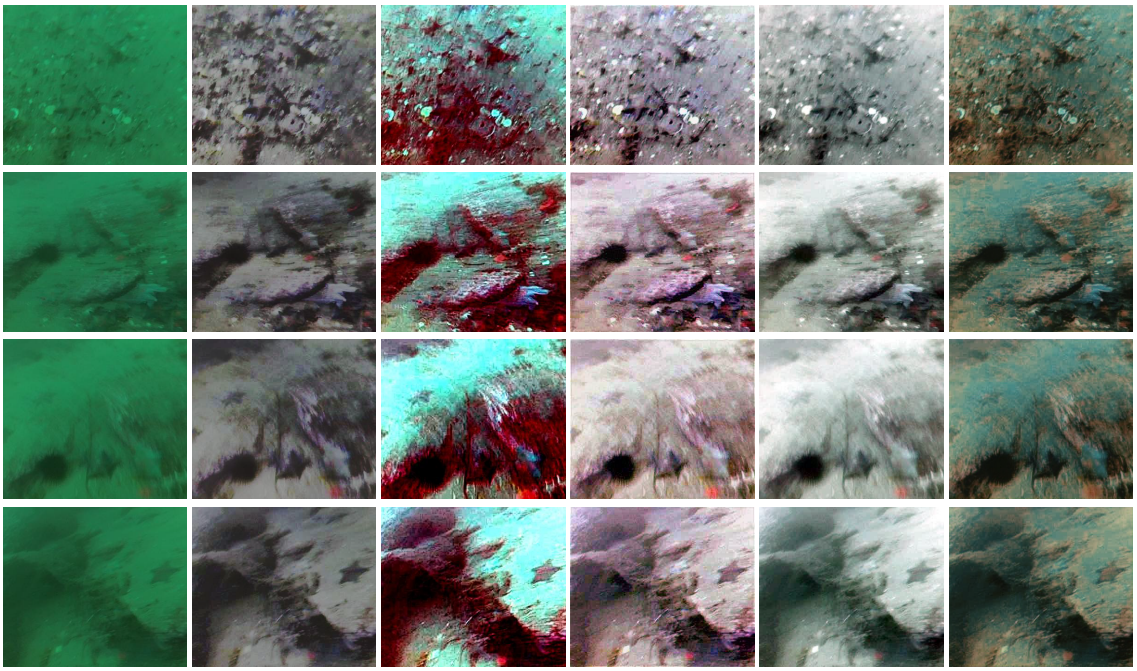

(a) Input (b) Fusion [51] (c) HLRP [32] (d) ACDC [52] (e) Improved-Retinex [49] (f) Hybrid model

Figure 3: Visual results: (**a**) original underwater images (RIE UCCS (green)) (**b**) fusion [51] (**c**) HLRP [32] (**d**) ACDC [52] (**e**) improved-retinex [49] (**f**) the hybrid model.

To further evaluate perceptual restoration quality, we additionally report Fréchet Inception Distance (FID), Single Image Fréchet Inception Distance (SIFID) [63], Clean-FID [64], and Learned Perceptual Image Patch Similarity (LPIPS) [65] on the UIEB-T90 dataset, as summarized in Table 1. The proposed Hybrid model achieves competitive perceptual performance, obtaining the second-best SIFID and the third-best LPIPS among the compared methods. Although some recent methods achieve lower FID or Clean-FID values, the proposed method demonstrates a balanced trade-off between perceptual similarity and conventional quantitative quality metrics, which is also consistent with the visual comparisons.

Regarding the performance evaluation in terms of quantitative results, there are two types of objective image quality assessment (QA) parameters in the literature that are known as full-reference and non-reference metrics. The full-reference metrics include the structure similarity index measure (SSIM) and peak signal-to-noise ratio (PSNR), which are used in cases where the ground truth images are available. Whereas, the non-reference parameters are underwater image quality metric (UIQM), UCIQE, visual contrast measure (VCM), image visibility measurement (IVM) and enhancement ratio of visible edges denoted as e are used where paired images in datasets are not available [21]. In order to evaluate our proposed model on UIEB-T90 datasets (which is paired datasets) we use the SSIM and PSNR metrics as these datasets provide ground truth images. The SSIM finds the similarity between a reference image x and the restored image y as:

$$SSIM(x, y) = \frac{(2\mu_x\mu_y + C_1)(2\sigma_{xy} + C_2)}{(\mu_x^2 + \mu_y^2 + C_1)(\sigma_x^2 + \sigma_y^2 + C_2)}, \tag{17}$$

where μ_x and μ_y are the average luminances of image x and image y, respectively. While $\sigma^2_{(.)}$ is the variance, and the σ_{xy} is the covariance between the reference and restored images. The C_1 and C_2 are very small constants used to stabilize the division process.

The PSNR quantifies the ratio between the maximum possible power of the reference image and the power of the restored image. On UIEB-T90, proposed model attains the highest reference-based fidelity with SSIM 0.892 and PSNR 21.49, outperforming the recent state-of-the-art methods, including CCL-Net and OUNet- JL, underscoring the advantage of our proposed hybrid model for jointly preserving structure and accurate color/contrast.

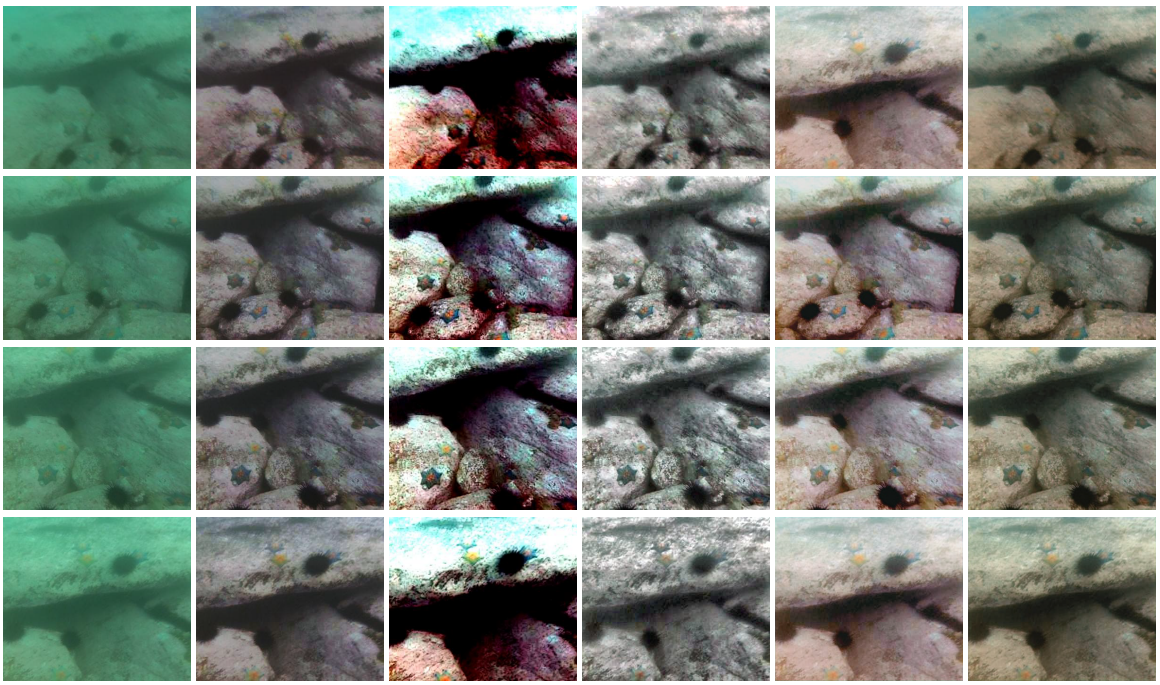

(a) Input (b) Fusion [51] (c) HLRP [32] (d) ACDC [52] (e) WaterNet [22] (f)Hybrid model

Figure 4: Visual results: (**a**) original underwater images (RIE UCCS (blue-green)) (**b**) fusion [51] (**c**) HLRP [32] (**d**) ACDC [52] (**e**) WaterNet [22] (**f**) the hybrid model.

Higher values of PSNR indicate better quality and are calculated as:

$$\text{PSNR} = 10 \cdot \log_{10}\left(\frac{R^2}{\text{MSE}}\right),$$

where R is the maximum possible value of pixels, whereas MSE is the mean squared error (MSE) between the original (reference) image and the enhanced image. It quantifies the average squared differences between corresponding pixel values and is computed as:

$$\text{MSE} = \frac{1}{N}\sum_{i=1}^{N}(x_i - y_i)^2,$$

where N is the total number of pixels, x_i and y_i are the pixel values of the reference and restored images, respectively. For further details of SSIM, PSNR, and MSE, we refer to [66].

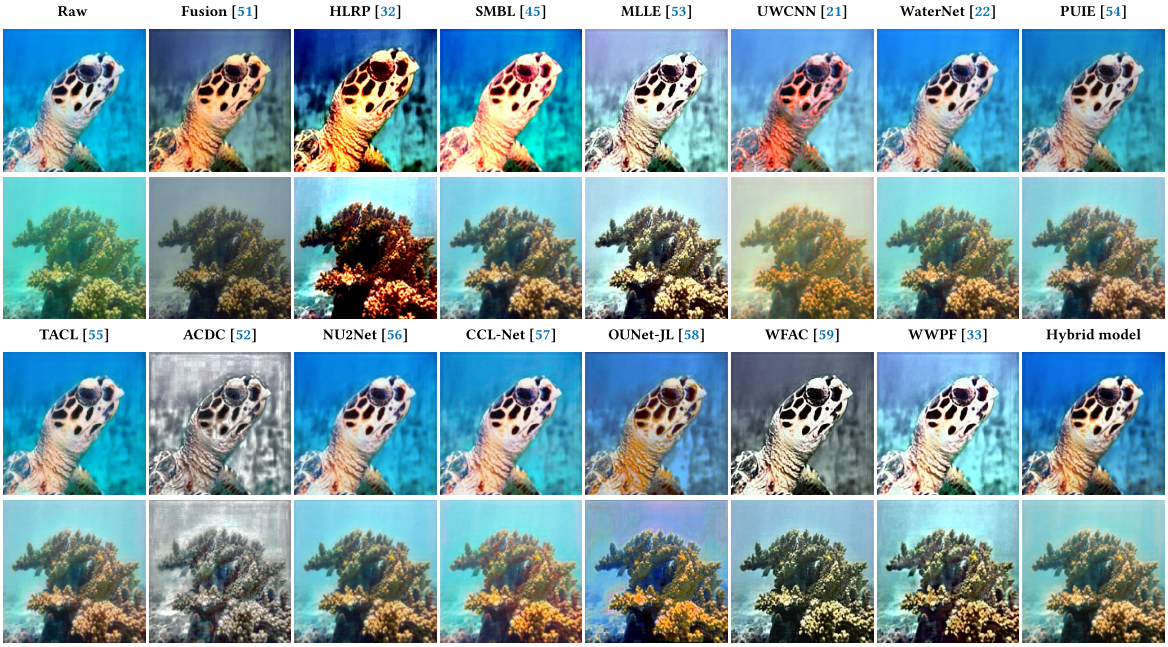

Figure 5: Comparison on the EUVP-T515 dataset using two samples with greenish and bluish color casts. The columns show the raw input, fusion [51], HLRP [32], SMBL [45], MLLE [53], UWCNN [21], WaterNet [22], PUIE [54], TACL [55], ACDC [52], NU2Net [56], CCL-Net [57], OUNet-JL [58], WFAC [59], WWPF [33], and the proposed hybrid model.

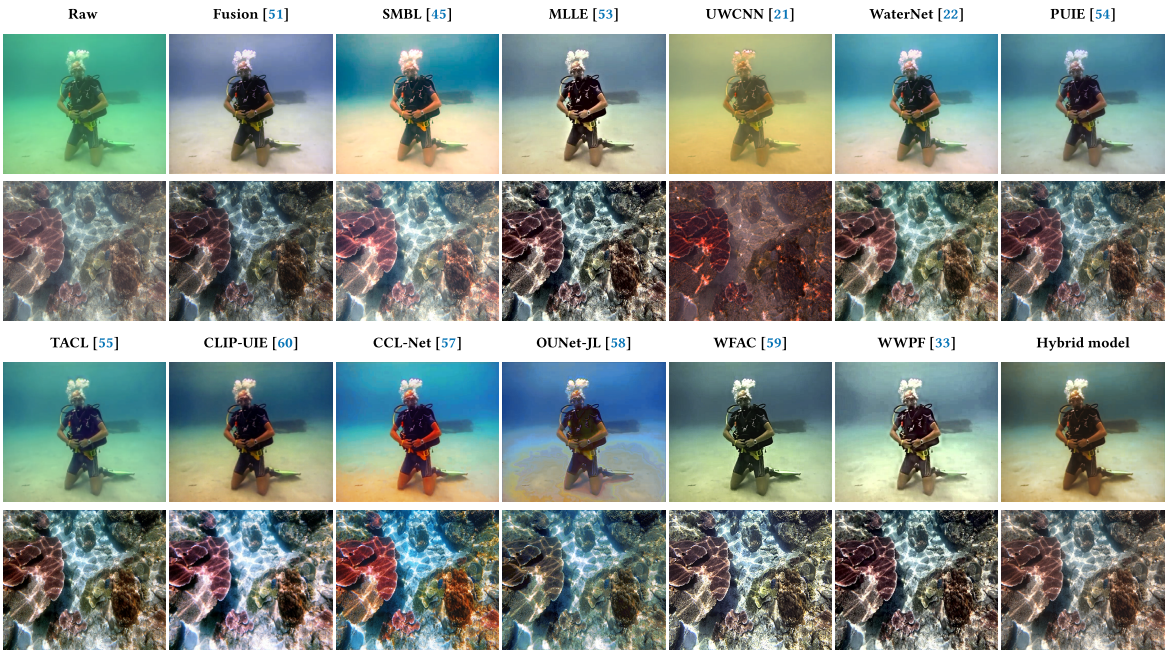

Figure 6: Comparison on the UIEB-T90 dataset using two samples with greenish and bluish color casts. The columns show the raw input, fusion [51], SMBL [45], MLLE [53], UWCNN [21], WaterNet [22], PUIE [54], TACL [55], CLIP-UIE [60], CCL-Net [57], OUNet-JL [58], WFAC [59], WWPF [33], and the proposed hybrid model.

(a) Input (b) Fusion [51] (c) U-Shape [61] (d) CCL-Net[57] (e) OUNet-JL [58] (f) WFAC [59] (g) Proposed

Figure 7: Subjective visual comparison on the UIEB Challenging-T60 dataset. The columns show the input image, fusion [51], U-shape [61], CCL-Net [57], OUNet-JL [58], WFAC [59], and the proposed hybrid model.

Table 1: Perceptual quality is evaluated on the UIEB-T90 dataset using FID, SIFID, Clean-FID, and LPIPS. Lower values mean better perceptual similarity. The best, second-best, and third-best results are shown in red, green, and blue, respectively. The symbol ↓ indicates that lower metric values are better.

Methods	FID↓	SIFID↓	Clean-FID↓	LPIPS↓
Fusion [51]	37.60	0.826	32.72	0.197
SMBL [45]	41.76	1.120	47.30	0.275
MLLE [53]	55.72	2.353	48.03	0.310
WWPF [33]	51.18	1.318	52.62	0.253
WFAC [59]	55.86	2.982	48.92	0.366
UWCNN [21]	93.47	2.173	94.00	0.377
WaterNet [22]	23.25	0.583	27.61	0.142
PUIE [54]	18.85	0.524	24.73	0.122
TACL [55]	25.31	0.559	30.71	0.192
NU2Net [56]	25.94	0.653	32.86	0.179
CCL-Net [57]	28.65	0.571	37.84	0.185
Hybrid Model	27.56	0.553	33.71	0.155

The RIE, RUIE, and EUVIP (unpaired datasets) do not provide ground truth images, for which we use the non-reference metrics e, IVM, VCM, and $UIQM$ also used in [3,13,47]. Note that the quality metric $UIQM$ further involves three metrics: the underwater image colorfulness measure ($UICM$), the underwater image sharpness measure ($UISM$), and the underwater image contrast measure ($UIConM$) in a linear combination, and is given as

$$UIQM = c1 \times UICM + c2 \times UISM + c3 \times UIConM, \tag{18}$$

where $c1$, $c2$ and $c3$ are the scale parameters. In our experiments we set $c1 = 0.0282$, $c2 = 0.2953$, and $c3 = 3.5753$ following the Panetta et al. [67]. Expressions involved in calculating the $UICM$, $UISM$, and $UIConM$ can be found in [67]. The UIQM and UCIQE values for the UIEB-C60, EUVP-T515, and RUIE-T78 datasets are reported in Table 2. The best, second-best, and third-best results are highlighted in red, green, and blue, respectively. As shown in the table, the proposed hybrid model outperforms competing methods on all

evaluated datasets, with the exception of UIEB-C60. The enhancement ratio of visible edges of the restored UWIs is given as

$$e = \left(\frac{n_j - n_k}{n_k} \right), \tag{19}$$

where n_j and n_k represent the cardinal number of visible edges in the original and the restored underwater images, respectively. The greater values of e indicate that the edges of the image are better restored.

Table 2: Quantitative results on UIEB-C60, EUVP-T515, and RUIE-T78 using UIQM and UCIQE. The best, second-best, and third-best scores are highlighted in red, green, and blue, respectively. The symbol ↑ indicates that higher metric values are better.

Methods	UIEB-C60		EUVP-T515		RUIE-T78	
	UIQM↑	UCIQE↑	UIQM↑	UCIQE↑	UIQM↑	UCIQE↑
Raw	1.856	0.359	2.217	0.417	2.437	0.321
Fusion [51]	2.163	0.378	2.636	0.430	2.772	0.366
SMBL [45]	1.724	0.439	1.857	0.513	2.459	0.431
MLLE [53]	1.956	0.464	2.354	0.461	2.798	0.441
UWCNN [21]	2.433	0.340	2.822	0.369	3.053	0.314
WaterNet [22]	2.468	0.364	2.680	0.412	3.115	0.403
UColor [41]	2.411	0.371	2.749	0.404	3.006	0.345
PUIE [54]	2.379	0.375	2.748	0.407	2.989	0.379
TACL [55]	2.854	0.424	2.837	0.435	3.237	0.422
NU2Net [56]	2.508	0.402	2.767	0.422	3.061	0.389
CCL-Net [57]	2.622	0.434	2.936	0.456	3.168	0.447
OUNet-JL [58]	2.842	0.426	3.107	0.436	3.212	0.425
Hybrid Model	2.280	0.565	4.33	0.612	3.88	0.553

For the paired datasets of UIEB-T90, the SSIM values of the proposed hybrid model and some of the existing are given in Table 3 where the first three higher values are shown as red, green and blue. Note that the higher value of the SSIM depicts the higher closeness of the restored UWIs with the reference images. The Table 4 provides the on average quantitative results in terms of non-reference metrics for the RIE UCCS (blue, green, and blue-green) dataset. The best-performing results for each metric and dataset category are highlighted in bold. Since higher values of e, IVM, VCM, and UIQM indicate better restoration quality, the bold entries identify the method achieving the highest score for the corresponding metric and dataset. Note that the higher value of IVM means a better restored image visibility, whereas the corresponding VCM value quantifies in terms of degree. Table 4 shows that the proposed approach achieves a higher value of IVM and VCM as compared to the other approaches in most of the cases. The quantitative evaluation and its comparison with the existing approaches confirm that the proposed approach achieves clearer visibility in restoring the underwater images. In literature, we note that although some of the conventional techniques based on physical models provide valuable performance but are found to be poor regarding the generalization of results [68]. Similarly, the deep learning-based techniques struggle for satisfactory results due to the lack of paired datasets in the case of UWIs [41]. The proposed model provides satisfactory restoration results and generalizes well in the case of diverse datasets of UWIs used in our experimental evaluation. In our work, the preprocessing of UWIs using the diverse techniques: CLAHE, GC, SSR, PM, and the further processing in a

parameterized learning framework with interactive scaling of processed results, generalizes the performance of the proposed model.

Table 3: Quantitative results on the UIEB dataset using PSNR, SSIM, UIQM, and UCIQE. The best, second-best, and third-best values are highlighted in red, green, and blue, respectively. The symbol ↑ indicates that higher metric values are better.

Methods	PSNR↑	SSIM↑	UIQM↑	UCIQE↑
Raw	16.134	0.748	2.346	0.362
Fusion [51]	18.033	0.861	2.684	0.406
SMBL [45]	16.513	0.781	2.167	0.455
MLLE [53]	18.727	0.790	2.305	0.468
WWPF [33]	19.260	0.805	2.566	0.408
WFAC [59]	17.540	0.748	2.581	0.372
UWCNN [21]	18.147	0.847	2.878	0.357
WaterNet [22]	19.914	0.859	2.846	0.410
UColor [41]	20.933	0.869	2.869	0.391
TACL [55]	22.735	0.864	3.016	0.445
CCL-Net [57]	20.181	0.866	3.021	0.464
OUNet-JL [58]	19.541	0.829	3.340	0.442
Hybrid Model	21.49	0.892	4.258	0.594

Table 4: Quantitative comparison in terms of the objective quality assessment metrics e, IVM, VCM, and UIQM for the restored RIE UCCS (blue, green, and blue-green) dataset.

QA index	Dataset	Fusion [51]	ACDC [52]	WaterNet [22]	Hybrid
e	UCCS (blue)	8.81	4.85	7.66	**9.08**
IVM		6.78	5.76	6.56	**6.79**
VCM		**60.35**	52.00	61.45	58.20
UIQM		3.66	3.66	3.12	**3.68**
e	UCCS (green)	20.26	14.21	15.57	**22.97**
IVM		4.83	3.61	3.89	**5.20**
VCM		**39.96**	37.56	44.26	38.30
UIQM		3.63	3.07	3.57	**3.68**
e	UCCS (blue-green)	16.41	**25.76**	15.93	15.79
IVM		4.03	**5.91**	3.89	3.80
VCM		40.42	**64.57**	44.26	40.15
UIQM		3.48	4.09	3.43	**4.66**

5.1 Ablation Study

To evaluate the contribution of the main components of the proposed framework, we conduct an ablation study on the UIEB-T90 paired test set. We progressively analyze the effect of the preprocessing branches and compare them with the full hybrid model. Specifically, we evaluate CLAHE+GC+SSR, HE+GC,

HE, HE+GC+RPM, and HE+RPM, and compare them with the full hybrid model. Fig. 8 presents qualitative comparisons of representative restored underwater images obtained by different configurations. The results show that CLAHE improves local contrast, but the restored images still suffer from limited color correction. Adding gamma correction improves brightness adjustment in some regions, while the inclusion of SSR further enhances reflectance-related details and visibility. However, these reduced configurations still exhibit insufficient restoration in severely degraded regions. In contrast, the Full Hybrid Model produces more balanced color correction, improved visibility, and better structural preservation. This improvement is attributed to the integration of the RUIFM-based physical restoration branch and the proposed physically guided fusion mechanism, which allows physically restored information to guide the remaining enhancement branches. The best-performing quantitative results for each metric are highlighted in bold and reported in Table 5. Since higher PSNR, SSIM, UIQM, and UCIQE values indicate better restoration quality, the bold entries identify the best-performing ablation configuration for each metric. The inclusion of the physical model branch (RPM) consistently improves all evaluation metrics across different enhancement strategies. Notably, the combination of the full model Hybrid model (CLAHE+GC+SSR with RPM) achieves the best performance, demonstrating the effectiveness of hybrid guidance in preserving structural details and enhancing perceptual quality.

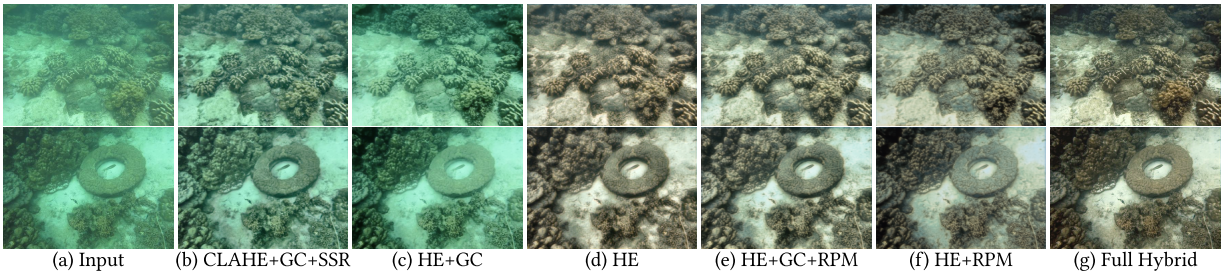

Figure 8: Qualitative ablation results on the UIEB-T90 dataset. Columns show: (**a**) input image, (**b**) CLAHE+GC+SSR, (**c**) HE+GC, (**d**) HE, (**e**) HE+GC+RPM, (**f**) HE+RPM, and (**g**) the full hybrid model.

Table 5: Ablation study and baseline comparison on the UIEB-T90 paired test dataset. The symbol ↑ indicates that higher metric values are better.

Method	PSNR ↑	SSIM ↑	UIQM ↑	UCIQE ↑
CLAHE+GC+SSR	17.84	0.73	3.09	0.29
HE+GC	18.18	0.70	2.34	0.34
HE	18.42	0.73	3.24	0.29
HE+GC+RPM	18.39	0.72	3.28	0.29
HE+RPM	19.25	0.72	3.21	0.32
Full hybrid model	**21.49**	**0.89**	**4.25**	**0.59**

6 Conclusion

Although the UWI enhancement techniques based on physical and nonphysical models, the CNNs using the physical model, and the CNNs not using the physical models, perform well but are not able to deal with the restoration and enhancement of UWIs captured in diverse environments independently. In this work, we present a framework that investigates and unifies the strength of each category of techniques. We use the nonphysical model-based techniques, the CLAHE, GC and SSR, and achieve to overcome the

low visibility and color degradation. While we use the revised physical model to achieve restoration and preserve under- and over-enhancement in the case of UWI. The processed images of the aforementioned techniques are used to train a CNN and an FTN network. The qualitative and quantitative performance of the proposed approach on the publicly available challenging datasets confirms its improved generalization and effectiveness. However, these techniques are currently employed only as preprocessing steps, and their parameters are not learned within the CNN or FTN framework. This separation limits the model's ability to fully adapt to diverse underwater conditions. In future work, we plan to integrate these preprocessing operations directly into the CNN architecture, enabling end-to-end learning of the associated parameters. Such an approach is expected to improve the network's adaptability across varying environments and enhance the overall generalization capability of the hybrid model.

Acknowledgement: We would like to express our gratitude to the School of Electronic Engineering and Intelligent Manufacturing, Anhui Xinhua University, Hefei, China, for providing academic guidance and technical support during this study.

Funding Statement: This work is supported by the National Natural Science Foundation of China under Grant No. W2433153, Anhui Provincial Department of Education Natural Science Research Project under Grant No. 2025AHGXZK31529, Key Project of the School of Electronic Engineering and Intelligent Manufacturing, Anhui Xinhua University under Grant No. 2025zrzdi06, and Anhui Xinhua University Research Start-Up Fund for Young Doctoral Research under Grant No. 2026kyqd18.

Author Contributions: The authors confirm their contributions to the paper as follows: study conception and design: Sami Ullah, Najmul Hassan and Naeem Bhatti; methodology: Sami Ullah, Najmul Hassan and Naeem Bhatti; implementation and experiments: Sami Ullah and Najmul Hassan; analysis and interpretation of results: Sami Ullah, Najmul Hassan, Naeem Bhatti and Asad Saleem; draft manuscript preparation: Sami Ullah and Najmul Hassan; review and editing: Naeem Bhatti and Asad Saleem. All authors reviewed and approved the final version of the manuscript.

Availability of Data and Materials: Availability of Data and Materials: The datasets used in this study are publicly available. The UIEB dataset is available at http://smartdsp.xmu.edu.cn/underwater.html, the EUVP dataset is available at https://irvlab.dl.umn.edu/resources/euvp-dataset, and the RUIE dataset is available at https://github.com/agaldran/UnderWater. No new dataset was generated in this study.

Ethics Approval: Not applicable.

Conflicts of Interest: The authors declare no conflicts of interest.

References

1. Ali M, Hassan N, Ventura L, Di Bari D, Canese S. AQUA-Net: adaptive frequency fusion and illumination aware network for underwater image enhancement. arXiv:2512.05960. 2025.
2. He K, Sun J, Tang X. Single image haze removal using dark channel prior. IEEE Trans Pattern Anal Mach Intell. 2010;33(12):2341–53. doi:10.1109/tpami.2010.168.
3. Galdran A, Pardo D, Picón A, Alvarez-Gila A. Automatic red-channel underwater image restoration. J Vis Commun Image Represent. 2015;26(4):132–45. doi:10.1016/j.jvcir.2014.11.006.
4. Drews PL, Nascimento ER, Botelho SS, Campos MFM. Underwater depth estimation and image restoration based on single images. IEEE Comput Graph Appl. 2016;36(2):24–35. doi:10.1109/mcg.2016.26.
5. Liang Z, Wang Y, Ding X, Mi Z, Fu X. Single underwater image enhancement by attenuation map guided color correction and detail preserved dehazing. Neurocomputing. 2021;425(4):160–72. doi:10.1016/j.neucom.2020.03.091.
6. Hummel R. Image enhancement by histogram transformation. Comput Graph Image Process. 1977;6(2):184–95. doi:10.1016/s0146-664x(77)80011-7.

7. Reza AM. Realization of the contrast limited adaptive histogram equalization (CLAHE) for real-time image enhancement. J VLSI Signal Process Syst Signal Image Video Technol. 2004;38(1):35–44. doi:10.1023/b:vlsi.0000028532.53893.82.
8. Ghani ASA, Isa NAM. Underwater image quality enhancement through integrated color model with Rayleigh distribution. Appl Soft Comput. 2015;27:219–30. doi:10.1016/j.asoc.2014.11.020.
9. Iqbal K, Odetayo M, James A, Salam RA, Talib AZH. Enhancing the low quality images using unsupervised colour correction method. In: Proceedings of the 2010 IEEE International Conference on Systems, Man and Cybernetics; 2010 Oct 10–13; Istanbul, Turkey. p. 1703–9.
10. Ancuti CO, Ancuti C, De Vleeschouwer C, Sbert M. Color channel compensation (3C): a fundamental pre-processing step for image enhancement. IEEE Trans Image Process. 2019;29:2653–65.
11. Zhuang P, Li C, Wu J. Bayesian retinex underwater image enhancement. Eng Appl Artif Intell. 2021;101(1):104171. doi:10.1016/j.engappai.2021.104171.
12. Liu R, Ma L, Zhang J, Fan X, Luo Z. Retinex-inspired unrolling with cooperative prior architecture search for low-light image enhancement. In: Proceedings of the 2021 IEEE/CVF Conference on Computer Vision and Pattern Recognition; 2021 Jun 20–25; Nashville, TN, USA. p. 10561–70.
13. Hassan N, Ullah S, Bhatti N, Mahmood H, Zia M. The retinex-based improved underwater image enhancement. Multimed Tools Appl. 2021;80(2):1839–57. doi:10.1007/s11042-020-09752-2.
14. Dong L, Zhang W, Xu W. Underwater image enhancement via integrated RGB and LAB color models. Signal Process Image Commun. 2022;104(12):116684. doi:10.1016/j.image.2022.116684.
15. Ghani ASA, Isa NAM. Automatic system for improving underwater image contrast and color through recursive adaptive histogram modification. Comput Electron Agric. 2017;141(4):181–95. doi:10.1016/j.compag.2017.07.021.
16. Ancuti C, Ancuti CO, Haber T, Bekaert P. Enhancing underwater images and videos by fusion. In: Proceedings of the 2012 IEEE Conference on Computer Vision and Pattern Recognition; 2012 Jun 16–21; Providence, RI, USA. p. 81–8.
17. Guo P, Zeng D, Tian Y, Liu S, Liu H, Li D. Multi-scale enhancement fusion for underwater sea cucumber images based on human visual system modelling. Comput Electron Agric. 2020;175:105608. doi:10.1016/j.compag.2020.105608.
18. Fu X, Zhuang P, Huang Y, Liao Y, Zhang XP, Ding X. A retinex-based enhancing approach for single underwater image. In: Proceedings of the 2014 IEEE International Conference on Image Processing (ICIP); 2014 Oct 27–30; Paris, France. p. 4572–6.
19. Li CY, Guo JC, Cong RM, Pang YW, Wang B. Underwater image enhancement by dehazing with minimum information loss and histogram distribution prior. IEEE Trans Image Process. 2016;25(12):5664–77. doi:10.1109/tip.2016.2612882.
20. Li J, Skinner KA, Eustice RM, Johnson-Roberson M. WaterGAN: unsupervised generative network to enable real-time color correction of monocular underwater images. IEEE Robot Autom Lett. 2017;3(1):387–94. doi:10.1109/lra.2017.2730363.
21. Li C, Anwar S, Porikli F. Underwater scene prior inspired deep underwater image and video enhancement. Pattern Recognit. 2020;98(1):107038. doi:10.1016/j.patcog.2019.107038.
22. Li C, Guo C, Ren W, Cong R, Hou J, Kwong S, et al. An underwater image enhancement benchmark dataset and beyond. IEEE Trans Image Process. 2019;29:4376–89. doi:10.1109/tip.2019.2955241.
23. Zhou J, Yang T, Chu W, Zhang W. Underwater image restoration via backscatter pixel prior and color compensation. Eng Appl Artif Intell. 2022;111:104785. doi:10.1016/j.engappai.2022.104785.
24. Wang Y, Liu H, Chau LP. Single underwater image restoration using adaptive attenuation-curve prior. IEEE Trans Circuits Syst I Regul Pap. 2017;65(3):992–1002. doi:10.1109/tcsi.2017.2751671.
25. Berman D, Levy D, Avidan S, Treibitz T. Underwater single image color restoration using haze-lines and a new quantitative dataset. IEEE Trans Pattern Anal Mach Intell. 2020;43(8):2822–37. doi:10.1109/tpami.2020.2977624.
26. Yuan J, Cai Z, Cao W. TEBCF: real-world underwater image texture enhancement model based on blurriness and color fusion. IEEE Trans Geosci Remote Sens. 2021;60:1–15.

27. Peng YT, Cosman PC. Underwater image restoration based on image blurriness and light absorption. IEEE Trans Image Process. 2017;26(4):1579–94. doi:10.1109/tip.2017.2663846.
28. Akkaynak D, Treibitz T. A revised underwater image formation model. In: Proceedings of the 2018 IEEE/CVF Conference on Computer Vision and Pattern Recognition; 2018 Jun 18–23; Salt Lake City, UT, USA. p. 6723–32.
29. Ullah S, Hassan N, Bhatti N. A diverse underwater image formation model for underwater image restoration. Earth Sci Inform. 2024;17(6):5371–83. doi:10.1007/s12145-024-01462-9.
30. Wang Z, Shen L, Xu M, Yu M, Wang K, Lin Y. Domain adaptation for underwater image enhancement. IEEE Trans Image Process. 2023;32:1442–57.
31. Yuan J, Cao W, Cai Z, Su B. An underwater image vision enhancement algorithm based on contour bougie morphology. IEEE Trans Geosci Remote Sens. 2021;59(10):8117–28. doi:10.1109/tgrs.2020.3033407.
32. Zhuang P, Wu J, Porikli F, Li C. Underwater image enhancement with hyper-Laplacian reflectance priors. IEEE Trans Image Process. 2022;31(3):5442–55. doi:10.1109/tip.2022.3196546.
33. Zhang W, Zhou L, Zhuang P, Li G, Pan X, Zhao W, et al. Underwater image enhancement via weighted wavelet visual perception fusion. IEEE Trans Circuits Syst Video Technol. 2023;34(4):2469–83. doi:10.1109/tcsvt.2023.3299314.
34. Wang H, Zhang W, Ren P. Self-organized underwater image enhancement. ISPRS J Photogramm Remote Sens. 2024;215(1):1–14. doi:10.1016/j.isprsjprs.2024.06.019.
35. Ullah S, Bhatti N, Hassan N, Miah ASM, Nishimura S, Suzuki T, et al. Lightweight residual-aware physical model network for underwater image enhancement. In: Proceedings of the 2025 13th International Conference on Awareness Science and Technology (iCAST); 2025 Nov 19–21; Yogyakarta, Indonesia. p. 1–6.
36. Anwar S, Li C. Diving deeper into underwater image enhancement: a survey. Signal Process Image Commun. 2020;89(6):115978. doi:10.1016/j.image.2020.115978.
37. Guo Y, Li H, Zhuang P. Underwater image enhancement using a multiscale dense generative adversarial network. IEEE J Ocean Eng. 2019;45(3):862–70. doi:10.1109/joe.2019.2911447.
38. Liu X, Gao Z, Chen BM. IPMGAN: integrating physical model and generative adversarial network for underwater image enhancement. Neurocomputing. 2021;453:538–51.
39. Chang B, Yuan G, Li J. CDDU: convolutional dictionary deep unfolding network for underwater image enhancement. IEEE Trans Instrum Meas. 2025;74:1–18.
40. Fabbri C, Islam MJ, Sattar J. Enhancing underwater imagery using generative adversarial networks. In: Proceedings of the 2018 IEEE International Conference on Robotics and Automation (ICRA); 2018 May 21–25; Brisbane, Australia. p. 7159–65.
41. Li C, Anwar S, Hou J, Cong R, Guo C, Ren W. Underwater image enhancement via medium transmission-guided multi-color space embedding. IEEE Trans Image Process. 2021;30:4985–5000. doi:10.1109/tip.2021.3076367.
42. Islam MJ, Xia Y, Sattar J. Fast underwater image enhancement for improved visual perception. IEEE Robot Autom Lett. 2020;5(2):3227–34. doi:10.1109/lra.2020.2974710.
43. Yang M, Hu K, Du Y, Wei Z, Sheng Z, Hu J. Underwater image enhancement based on conditional generative adversarial network. Signal Process Image Commun. 2020;81(5):115723. doi:10.1016/j.image.2019.115723.
44. Chen X, Zhang P, Quan L, Yi C, Lu C. Underwater image enhancement based on deep learning and image formation model. arXiv:2101.00991. 2021.
45. Song W, Wang Y, Huang D, Liotta A, Perra C. Enhancement of underwater images with statistical model of background light and optimization of transmission map. IEEE Trans Broadcast. 2020;66(1):153–69. doi:10.1109/tbc.2019.2960942.
46. Kim JY, Kim LS, Hwang SH. An advanced contrast enhancement using partially overlapped sub-block histogram equalization. IEEE Trans Circuits Syst Video Technol. 2001;11(4):475–84. doi:10.1109/76.915354.
47. Hassan N, Ullah S, Bhatti N, Mahmood H, Zia M. A cascaded approach for image defogging based on physical and enhancement models. Signal Image Video Process. 2020;14(5):867–75. doi:10.1007/s11760-019-01618-x.
48. Ullah S, Hassan N, Bhatti N, Zia M, Shin J. White balancing based improved nighttime image dehazing. Multimed Tools Appl. 2024;84(1):445–62. doi:10.1007/s11042-024-18891-9.

49. Lin S, Li Z, Zheng F, Zhao Q, Li S. Underwater image enhancement based on adaptive color correction and improved retinex algorithm. IEEE Access. 2023;11(4):27620–30. doi:10.1109/access.2023.3258698.
50. Priyadharshini RA, Arivazhagan S, Pavithra K, Sowmya S. An ensemble deep learning approach for underwater image enhancement. e-Prime Adv Electr Eng Electron Energy. 2024;9(12):100634. doi:10.1016/j.prime.2024.100634.
51. Ancuti CO, Ancuti C, De Vleeschouwer C, Bekaert P. Color balance and fusion for underwater image enhancement. IEEE Trans Image Process. 2017;27(1):379–93. doi:10.1109/tip.2017.2759252.
52. Zhang W, Wang Y, Li C. Underwater image enhancement by attenuated color channel correction and detail preserved contrast enhancement. IEEE J Ocean Eng. 2022;47(3):718–35. doi:10.1109/joe.2022.3140563.
53. Zhang W, Zhuang P, Sun HH, Li G, Kwong S, Li C. Underwater image enhancement via minimal color loss and locally adaptive contrast enhancement. IEEE Trans Image Process. 2022;31:3997–4010. doi:10.1109/tip.2022.3177129.
54. Fu Z, Wang W, Huang Y, Ding X, Ma KK. Uncertainty inspired underwater image enhancement. In: European Conference on Computer Vision. Cham, Switzerland: Springer; 2022. p. 465–82.
55. Liu R, Jiang Z, Yang S, Fan X. Twin adversarial contrastive learning for underwater image enhancement and beyond. IEEE Trans Image Process. 2022;31:4922–36. doi:10.1109/tip.2022.3190209.
56. Guo C, Wu R, Jin X, Han L, Zhang W, Chai Z, et al. Underwater ranker: learn which is better and how to be better. Proc AAAI Conf Artif Intell. 2023;37(1):702–9.
57. Liu Y, Jiang Q, Wang X, Luo T, Zhou J. Underwater image enhancement with cascaded contrastive learning. IEEE Trans Multimed. 2024;27:1512–25. doi:10.1109/tmm.2024.3521739.
58. Wang X, Luo Z, Huang W, Zhang Y, Hu R. Optimized UNet framework with a joint loss function for underwater image enhancement. Sci Rep. 2025;15(1):7327. doi:10.1038/s41598-025-91839-7.
59. Zhang W, Liu Q, Lu H, Wang J, Liang J. Underwater image enhancement via wavelet decomposition fusion of advantage contrast. IEEE Trans Circuits Syst Video Technol. 2025;35(8):7807–20. doi:10.1109/tcsvt.2025.3545595.
60. Liu S, Li K, Ding Y, Qi Q. Underwater image enhancement by diffusion model with customized clip-classifier. Pattern Recognit. 2025;171(6):112232. doi:10.1016/j.patcog.2025.112232.
61. Peng L, Zhu C, Bian L. U-shape transformer for underwater image enhancement. IEEE Trans Image Process. 2023;32(2):3066–79. doi:10.1109/tip.2023.3276332.
62. Liu R, Fan X, Zhu M, Hou M, Luo Z. Real-world underwater enhancement: challenges, benchmarks, and solutions under natural light. IEEE Trans Circuits Syst Video Technol. 2020;30(12):4861–75.
63. Shaham TR, Dekel T, Michaeli T. Singan: learning a generative model from a single natural image. In: Proceedings of the 2019 IEEE/CVF International Conference on Computer Vision; 2019 Oct 27–Nov 2; Seoul, Republic of Korea. p. 4570–80.
64. Parmar G, Zhang R, Zhu JY. On aliased resizing and surprising subtleties in GAN evaluation. In: Proceedings of the 2022 IEEE/CVF Conference on Computer Vision and Pattern Recognition; 2022 Jun 18–24; New Orleans, LA, USA. p. 11410–20.
65. Zhang R, Isola P, Efros AA, Shechtman E, Wang O. The unreasonable effectiveness of deep features as a perceptual metric. In: Proceedings of the IEEE Conference on Computer Vision and Pattern Recognition; 2018 Jun 18–23; Salt Lake City, UT, USA. p. 586–95.
66. Wang Z, Bovik AC, Sheikh HR, Simoncelli EP. Image quality assessment: from error visibility to structural similarity. IEEE Trans Image Process. 2004;13(4):600–12. doi:10.1109/tip.2003.819861.
67. Panetta K, Gao C, Agaian S. Human-visual-system-inspired underwater image quality measures. IEEE J Ocean Eng. 2015;41(3):541–51. doi:10.1109/joe.2015.2469915.
68. Wang H, Sun S, Ren P. Meta underwater camera: a smart protocol for underwater image enhancement. ISPRS J Photogramm Remote Sens. 2023;195:462–81.